A&A 440, 1087–1095 (2005)
DOI: 10.1051/0004-6361:20053174

Astronomy & Astrophysics

Binaries discovered by the SPY project

IV. Five single-lined DA double white dwarfs⋆,⋆⋆,⋆⋆⋆,†

G. Nelemans[1,2], R. Napiwotzki[3], C. Karl[4], T. R. Marsh[5], B. Voss[6], G. Roelofs[1], R. G. Izzard[2,7], M. Montgomery[2], T. Reerink[8], N. Christlieb[9], and D. Reimers[9]

[1] Department of Astrophysics, Radboud University Nijmegen, PO Box 9010 6500 GL, Nijmegen, The Netherlands
e-mail: nelemans@astro.ru.nl
[2] Institute of Astronomy, University of Cambridge, Madingley Road, Cambridge CB3 0HA, UK
[3] Centre for Astrophysics Research, University of Hertfordshire, Hatfield, AL10 9AB, UK
[4] Remeis-Sternwarte, Universität Erlangen-Nürnberg, Sternwartestr. 7, 96049 Bamberg, Germany
[5] Department of Physics, University of Warwick, Coventry CV4 7AL, UK
[6] Institut für Theoretische Physik und Astrophysik, University of Kiel, 24098 Kiel, Germany
[7] The Carolune Institute for Quality Astronomy, www.ciqua.org, UK
[8] Astronomical Institute "Anton Pannekoek", University of Amsterdam, Kruislaan 403, 1098 SJ Amsterdam, The Netherlands
[9] Hamburger Sternwarte, Universität Hamburg, Gojensbergweg 112, 21029 Hamburg, Germany

Received 1 April 2005 / Accepted 6 June 2005

Abstract. We present results from our ongoing follow-up observations of double white dwarf binaries detected in the ESO SN Ia Progenitor SurveY (SPY). We discuss our observing strategy and data analysis and present the orbital solutions of five close double white dwarf binaries: HE0320−1917, HE1511−0448, WD0326−273, WD1013−010 and WD1210+140. Their periods range from 0.44 to 3.22 days. In none of these systems we find any spectral lines originating from the companion. This rules out main sequence companions and indicates that the companion white dwarfs are significantly older and cooler than the bright component. Infrared photometry suggests the presence of a cool, helium-rich white dwarf companion in the binary WD 0326−273. We briefly discuss the consequences of our findings for our understanding of the formation and evolution of double white dwarfs.

Key words. stars: binaries: close – stars: supernovae: general – stars: white dwarfs

1. Introduction

Most binaries in which the two components are close enough together to interact at some stage, will end their life as close double white dwarfs (e.g. Webbink 1984). They will experience at least two phases of mass transfer. In at least one of these phases, a so-called common envelope will be formed, in which the first formed white dwarf spirals into the envelope of its companion (e.g. Nelemans et al. 2001).

Although this population of close double white dwarfs was expected on theoretical grounds (Webbink 1984), it was only in 1988 that the first system was discovered (Saffer et al. 1988). In the 1990s the number of known systems increased to 18 (see Marsh 2000; Maxted et al. 2000a). Detailed knowledge of this population is important for a number of reasons. The observed double white dwarfs carry important information about the preceding binary evolution; in particular the mass ratio of the components reflects the change in orbital separation in the mass transfer phases and puts constraints on the physics and applicability of the common envelope phase (Nelemans et al. 2000). Furthermore double white dwarfs are so abundant that they form an important background for gravitational wave radiation experiments like LISA, as well as being guaranteed detectable sources (e.g. Nelemans et al. 2004). Last but not least double white dwarfs play an important role in the still ongoing debate on, or rather quest for, the nature of the progenitors of type Ia supernovae.

⋆ Based on observations made with the INT and WHT operated on the island of La Palma by the Isaac Newton Group in the Spanish Observatorio de Roque de los Muchachos of the Instituto de Astrophísica de Canarias.

⋆⋆ Based on observations at the Paranal and La Silla Observatories of the European Southern Observatory for program Nos. 165.H-0588, 167.D-0407, 68.D-0483, 69.D-0534, 70.D-0334, 71.D-0383.

⋆⋆⋆ Based on observations collected at the German-Spanish Astronomical Center (DSAZ), Calar Alto, operated by the Max-Planck-Institute für Astronomie jointly with the Spanish National Commission for Astronomy.

† Appendix A is only available in electronic form at http://www.edpsciences.org

Table 1. Overview of the follow-up observations, giving dates, telescopes, instruments and observers. For details of the set-ups of the different instruments, see text.

Date	Observatory	Telescope	Instrument	Observer
2001-03-10 to 13	Calar Alto	3.5 m	TWIN	R. Napiwotzki, E.-M. Pauli
2001-07-06 to 15	Calar Alto	3.5 m	TWIN	R. Napiwotzki, C. Karl
2001-10-11 to 12	Paranal	UT2	UVES	R. Napiwotzki
2001-10-26 to 01	La Palma	INT	IDS	G. Nelemans, T. Reerink
2002-02-22 to 26	Calar Alto	3.5 m	TWIN	C. Karl, T. Lisker
2002-06-04 to 05	Paranal	UT2	UVES	R. Napiwotzki
2002-08-11 to 16	Calar Alto	3.5 m	TWIN	C. Karl
2002-09-23 to 26	La Silla	NTT	EMMI	C. Karl
2002-10-15 to 16	Calar Alto	3.5 m	TWIN	C. Karl
2002-11-10 to 13	Paranal	UT2	UVES	R. Napiwotzki
2003-01-22 to 25	La Palma	WHT	ISIS	G. Nelemans, P. Groot
2003-02-17 to 21	La Silla	NTT	EMMI	C. Karl
2003-03-17 to 20	Paranal	UT2	UVES	R. Napiwotzki
2003-03-20 to 23	La Palma	WHT	ISIS	G. Nelemans, R. Izzard
2003-04-14 to 20	Calar Alto	3.5 m	TWIN	C. Karl
2003-05-13 to 18	Calar Alto	3.5 m	TWIN	C. Karl
2003-07-01 to 17	Calar Alto	3.5 m	TWIN	C. Karl
2003-08-06 to 09	La Palma	WHT	ISIS	G. Nelemans, M. Montgomery
2004-01-01 to 04	La Silla	NTT	EMMI	C. Karl
2004-11-27 to 01	La Silla	NTT	EMMI	C. Karl
2004-12-03 to 05	La Palma	WHT	ISIS	G. Roelofs
2004-12-25 to 30	La Palma	WHT	ISIS	G. Roelofs

Type Ia supernovae (SNe Ia) are among the best standard candles to determine the cosmological parameters (see Leibundgut 2001). Yet the nature of the SNe Ia progenitors remains unclear (see Livio 2001, for a review). One of the progenitor models is the merger of two white dwarfs (Iben & Tutukov 1984). Some explosion calculations show that merging double white dwarfs do *not* lead to an explosive event (e.g. Saio & Nomoto 1998) even when rotation is taken into account (Saio & Nomoto 2004), while other calculations including rotation do get explosions (Piersanti et al. 2003). The current explosion models are still too simplistic to rule out double white dwarfs as progenitors. For the use of SNe Ia as standard candles the nature of the progenitors is crucial (e.g. Hoeflich et al. 1998). One basic question that needs to be answered for any possible progenitor scenario is whether there are enough of them.

To give a definite answer to the question whether there exist enough merging double white dwarf with a mass above the Chandrasekhar limit we embarked on a spectroscopic survey of white dwarfs with the UVES spectrograph at the ESO-VLT (ESO SNIa Progenitor Survey, Napiwotzki et al. 2001a) and have observed more than 1000 white dwarfs (which corresponds to about 75 percent of the known white dwarfs accessible by the VLT with magnitudes brighter than $B = 16.5$). For each object we took two spectra to check for binarity, in order to provide good statistics of the double white dwarf population, including SN Ia progenitor candidates. A total of 875 stars were checked for radial velocity variations. SPY detected ≈100 new double white dwarfs (see Napiwotzki et al. 2004b). There are 16 double-lined systems and 18 non-DA white dwarf binaries. The sample furthermore turned out to be contaminated with some sdB stars, 31 of which are binaries (Napiwotzki et al. 2004a). The SPY project obtains 2 to 3 spectra per object, enough to determine its binarity and pick out the 1 in 10 or so white dwarfs that reside in a close binary. However, in order to obtain orbital solutions of all the binaries discovered in the SPY project, we started a systematic study of all new binaries, mainly with smaller telescopes. Earlier results were published in Napiwotzki et al. (2001b, 2002b); Karl et al. (2003). An overview of the follow-up observations up to Dec. 2004 is given in Table 1. In this paper we report results for the first five single-lined double white dwarfs for which we found the orbital solutions. Results on other types of binaries (double-lined systems and sdB binaries) will be presented in separate papers. In Sect. 2 we discuss our observations, data reduction and analysis, in Sect. 3 we present the orbital solutions for the five systems and in Sect. 5 we briefly compare our findings with population synthesis calculations.

2. Method

2.1. Observations and data reduction

Data were taken with a number of different telescope/ instrument combinations (see Table 1). The details of the different setups are as follows.

UT2/UVES: data taken with the UVES echelle spectrograph on UT2 of the 8.2 m Very Large Telescope of the European Southern Observatory at Paranal with the following setup: dichroic 1, central wavelengths 3900 and 5640 Å giving an almost full spectral coverage from 3200 to 6650 Å with two small (~80 Å) gaps around 4580 and 5640 Å. Slit widths varied between 1″ and 1.5″ for the follow-up observations and 2.1″ for the survey spectra, yielding a spectral resolution of 0.36 Å or better at Hα (see Napiwotzki et al. 2001a).

3.5 m/TWIN: data taken with the double arm TWIN spectrograph on the 3.5 m telescope at Calar Alto. Only data from the red arm are used in this paper. The setup consisted of the 230 mm camera with the T06 grating (1200 grooves mm^{-1}) and a SITe-CCD giving a dispersion of 0.55 Å/pix.

INT/IDS: data taken with the Intermediate Dispersion Spectrograph in the 2.5 m Isaac Newton Telescope on La Palma. The 500 mm camera with the 1200R grating centred on Hα was used, giving a dispersion of 0.39 Å/pix.

WHT/ISIS: data taken with the double arm ISIS spectrograph on the 4.2 m William Hershel Telescope on La Palma. Only data from the red arm are used in this paper. The setup was the 1200R grating centred on Hα, together with the MARCONI CCD giving a dispersion of 0.23 Å/pix.

NTT/EMMI: data taken with the EMMI spectrograph on the New Technology Telescope at La Silla in the red medium dispersion mode (REMD). We used grating #6, giving a dispersion of 0.2 Å/pix on the MLT/LL CCD.

Data reduction was done using standard IRAF or MIDAS tasks. Bias subtraction was done using the overscan region, while flatfielding was done using daytime dome flats. Spectra were extracted using optimal extraction, except for the survey spectra. Wavelength calibration is based on CuArNe arcs taken at the same position as the object before or after each exposure (for the IDS/ISIS data) and ArTh for the TWIN data. Details of the UVES data reduction will be described in a forthcoming paper on the SPY radial velocity catalogue (Napiwotzki et al., in prep.).

2.2. Radial velocity measurement and period determination

Based on previous experience we have used two different techniques of measuring the radial velocities of the white dwarfs.

The first is described in Napiwotzki et al. (2002b) and uses functions within the MIDAS context to fit a combination of a Gaussian plus a Lorentzian to the spectra. The radial velocities are calculated from the central wavelength of the fitted Gaussians. The velocities and observation times were later corrected to heliocentric values. In order to determine the orbital parameters radial velocity curves for a range of periods are fitted to produce a "power spectrum" indicating the fit quality as function of period.

We also used the technique developed by Marsh and collaborators, which utilizes a multi-Gaussian fitting technique to fit the shape of the spectral lines (see Marsh et al. 1995). A fixed template consisting of a number of different Gaussians (typically two or three), is fitted to the individual spectra in order to measure the radial velocity. A floating mean period search is used to find the orbital solution by minimizing the χ^2 of the fit of a sinusoidal curve to the radial velocity measurements (see Morales-Rueda et al. 2005, for a discussion of this technique). This yields the best fit period, radial velocity amplitude, velocity offset (in principle the system velocity, or γ-velocity, but not corrected for gravitational redshift), the zero-point (where the star moves from the blue to the red) and the mass function.

In order to cross check the two analysis methods we compared the resulting radial velocity measurements in detail for two binaries (HS1102+0934 and HS1102+0032, details of which will be published later) and found good agreement. Most values agree within 1 sigma, the maximum deviation was 1.44 sigma. All radial velocities presented in this paper are obtained with the second method.

Before discussing the individual objects we spend a few words on the error analysis. Following earlier practice with radial velocity data of double white dwarfs, we assume there are systematic errors of a few km s^{-1} that are due to imperfections in the setup. We therefore added 2 km s^{-1} quadratically to the errors that we obtain by propagating the errors on the spectra. We found that there were some additional errors that arise from combining data from different telescopes/instruments. We did not include any additional error term to account for this, but we chose to keep the errors as they are, which in some cases results in rather large values of χ^2. The errors on the derived quantities might thus be a bit optimistic. However, none of the derived periods is uncertain due to this effect.

3. Results

Table 2 summarizes the results for this first set of double white dwarfs. Listed are the orbital period ($P_{\rm orb}$), the radial velocity semi-amplitude (K), the system-velocity (γ), the zero-point (T_0, where the star moves from the blue to the red), the χ^2 of the fit, the number of data points (N), the difference of the χ^2 with the χ^2 of the second best fit period ($\Delta\chi^2$), the mass of the visible white dwarf (M_1) and the minimum mass of the companion white dwarf, from the mass function, M_1 and assuming an inclination of 90 degrees ($M_{2,\rm min}$).

The masses M_1 of the visible component were determined from a model atmosphere analysis of th UVES survey spectra (Voss et al. 2005, in prep.). In short, we determined temperature and surface gravity by fitting model spectra to the observed hydrogen Balmer lines of the DA white dwarfs. Depending on the temperature of the star we applied LTE or NLTE model atmospheres (cf. Koester et al. 2001, for a description). Finally we interpolated in the white dwarf cooling tracks of Benvenuto & Althaus (1999) to determine the mass. The results for the systems are discussed below individually.

Table 2. Overview of results of the follow-up observations. The columns give orbital period ($P_{\rm orb}$), the radial velocity semi-amplitude (K), the *gamma*-velocity (γ), the zero-point (T_0, where the star moves from the blue to the red), the χ^2 of the fit, the number of data points (N), the difference of the χ^2 with the χ^2 of the second best fit period ($\Delta\chi^2$), the mass of the visible white dwarf (M_1; from Voss et al. in prep.) and the minimum mass of the companion white dwarf, from the mass function, M_1 and assuming an inclination of 90 degrees ($M_{2,\rm min}$).

Object	$P_{\rm orb}$ (d)	K km s^{-1}	γ km s^{-1}	HJD (T_0) −2 400 000	χ^2	N	$\Delta\chi^2$	M_1 $M_\odot$	$M_{2,\rm min}$ $M_\odot$
HE0320−1917	0.86492(4)	105 ± 1	43 ± 1	52 658.97(5)	33.0	15	290	0.29	0.35
HE1511−0448	3.222(0)	74 ± 4	−36 ± 2	52 270.1(6)	12.9	15	31	0.48	0.46
WD0326−273	1.8754(5)	96.2 ± 0.5	70.0 ± 0.4	52 165.23(9)	69.8	39	1000	0.51	0.59
WD1013−010	0.43653(5)	122 ± 2	59 ± 1	53 016.41(1)	22.3	15	170	0.44	0.38
WD1210+140	0.64194(3)	131 ± 3	15 ± 2	52 170.29(4)	26.3	15	50	0.23	0.38

3.1. HE0320–1917

HE0320−1917 is relatively cool white dwarf of about 12 000 K, with a mass of 0.29 $M_\odot$. It was selected from the Hamburg/ESO survey (see Christlieb et al. 2001). The periodogram of HE0320−1917 is shown in Fig. 1. The best fit period is about 0.865 d (see Table 2). The radial velocity measurements folded on the best fit period are shown in Fig. 1. The minimum mass of the unseen companion is 0.35 $M_\odot$.

3.2. HE1511–0448

HE1511−0448 was again selected from the Hamburg/ESO survey and is a very hot white dwarfs (50 000 K), with a mass of 0.48 $M_\odot$. The line profile shows an emission core, so this object was fitted with three Gaussians, one for the emission core. The periodogram of HE1511−0448 is shown in Fig. 2. The orbital period is 3.22 days. There are two other solutions for the period (0.8 and 1.3 d), but they are very unlikely. The folded radial velocity curve is shown in Fig. 2.

3.3. WD0326–273

WD0326−273 (GJ 1060A, L 587−77A) was discovered by Luyten as a high proper motion white dwarf with an M(3.5) companion at ∼7 arcsec (e.g. Luyten 1949). The velocity difference of the two stars has been used to determine the gravitational redshift of the white dwarf (Koester 1987), yielding a mass of 0.65 $M_\odot$. Wegner & Reid (1991) on the other hand measured a blue shift and discarded that system as not physically associated. However, both these results are, of course, influenced by the orbital velocity.

Spectral fits to the SPY UVES spectra yield a mass of 0.46 $M_\odot$ (Voss et al. 2005, in prep.). Bergeron et al. (2001) find a mass of 0.35 $M_\odot$ based on photometric and parallax data, but a higher mass using spectroscopic mass determination. The analysis of the photometric data was flawed, because Bergeron et al. adopted $V = 14.0$, a value which can be traced back to a photographic measurement by Luyten (1957). A more accurate value ($y/V = 13.56$) is available from photoelectric observations in the Strömgren system by Bessell & Wickramasinghe (1978). We will discuss evidence for a remaining infrared excess below.

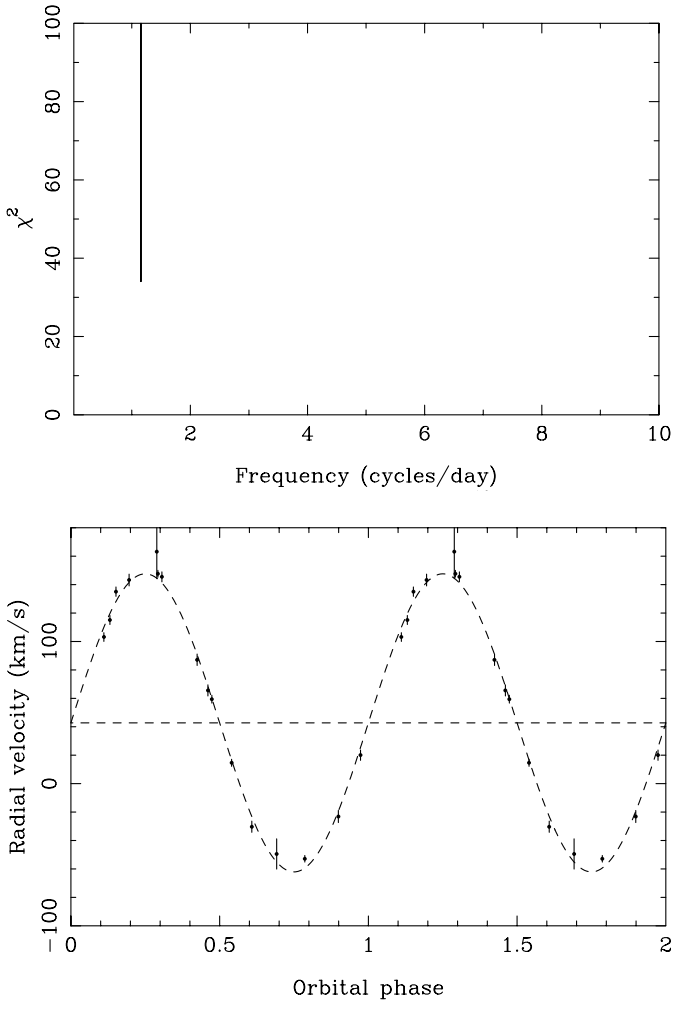

Fig. 1. *Top*: periodogram for HE0320−1917 showing the χ^2 as a function of the orbital period in cycles per day. Due to the availability of measurements over a long time span the χ^2 minima are so narrow that they appear as vertical lines. *Bottom*: the radial velocity data folded on the best fit period.

Gravitational redshift: with our orbital solution we are now in a position to determine the real gravitational redshift of the visible DA white dwarf. Due to a (fortunate) target confusion during the SPY survey observations one UVES spectrum of the M star companion L 587−77B was taken. The

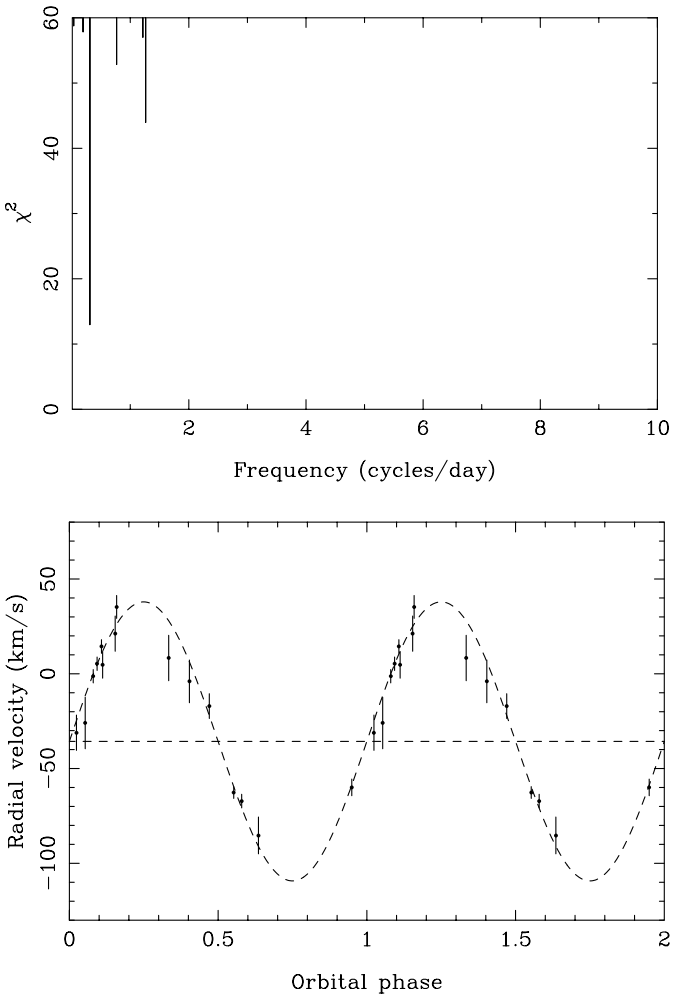

Fig. 2. Periodogram for HE1511−0448 in cycles per day (*top*) and data folded on the best fit period.

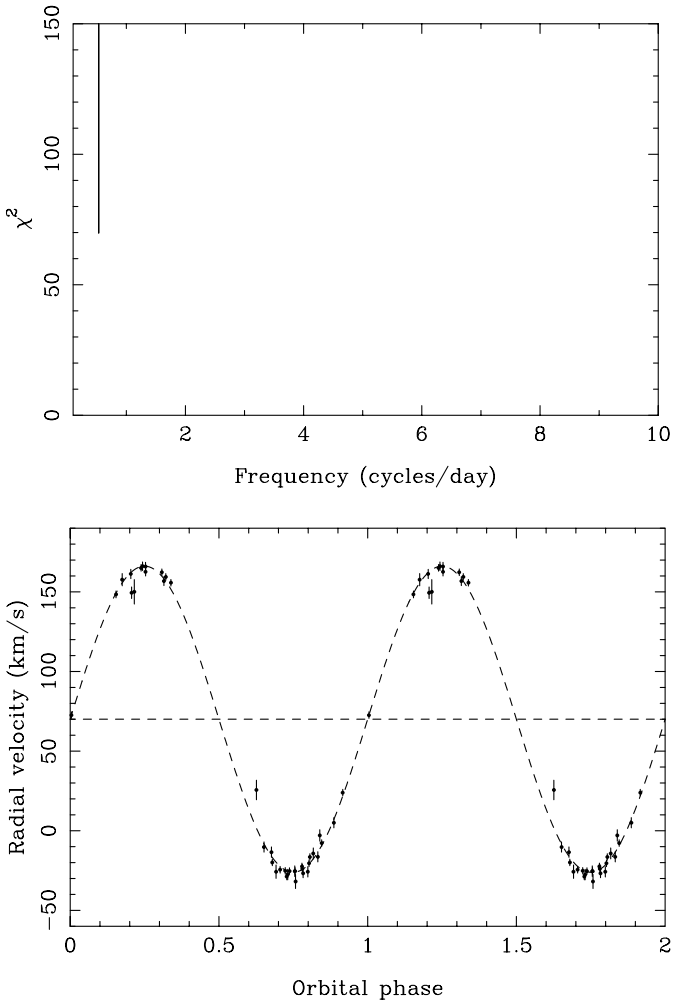

Fig. 3. Periodogram for WD0326−273 in cycles per day (*top*) and data folded on the best fit period.

Balmer lines are in emission and we measured the radial velocity from a simple Gaussian fits of the Hα and Hβ emissions. The measured value $v_{\rm Mstar} = 47 \pm 1\,{\rm km\,s^{-1}}$ translates into a redshift of $23\,{\rm km\,s^{-1}}$. Applying the white dwarf cooling tracks of Benvenuto & Althaus (1999) we derive a white mass of 0.51 $M_\odot$, slightly higher than the spectroscopic result. Let us note that taken at face value our radial velocity determination of the M dwarf is discrepant to the Wegner & Reid (1991) measurement of $v_{\rm Mstar} = 17 \pm 10\,{\rm km\,s^{-1}}$. However, the authors caution that the errors of their absolute radial velocity measurements are probably larger than the purely instrumental error.

The cool white dwarf companion: the quality of the model atmosphere fit of WD 0326−273 is inferior to the quality typically achievable for white dwarfs in this parameter range ($T_{\rm eff}$ = 9300 K, Voss et al. 2005, in prep.). Closer inspection of the optical and IR photometry revealed that a significant red/infrared excess is present (Fig. 4, top). A plausible explanation is a flux contribution from the apparently invisible cool white dwarf companion of the brighter DA. We collected the available photometric measurements (Strömgren b and y from Bessell & Wickramasinghe (1978); J, H, K from Bergeron et al. (2001); I and J from DENIS; J, H, K from 2MASS) and tried to fit these with a composite spectrum. We fixed the temperature of the bright DA component at the spectroscopic value of 9300 K and adopted equal masses for both white dwarfs. Synthetic absolute magnitudes and colours for pure hydrogen and pure helium atmospheres were taken from Bergeron et al. (1995). Fluxes were co-added and normalised to the measured V flux. A χ^2 analysis yielded a best fit for a helium-composed companion with a temperature $T_{\rm eff}$ = 6150±650 K (displayed in the bottom panel of Fig. 4). This corresponds to a featureless DC white dwarf. Fitting the colours for the hydrogen-rich models yielded a slightly worse fit at $T_{\rm eff} = 7300 \pm 350$ K. However, this solution can be ruled out, because it predicts a relatively strong Hα line for the secondary, which is clearly not present in the observed spectra (see Fig. 7).

The inner binary (assuming the M 3.5 star is physically associated in a very long period outer binary) has an orbital period of 1.88 d (Fig. 3). There are no other periods possible, given the relatively large number of spectra we have of this source. The large amplitude of the radial velocity curve shows that the companion star also has to be rather massive (more massive than 0.59 $M_\odot$, see Table 2).

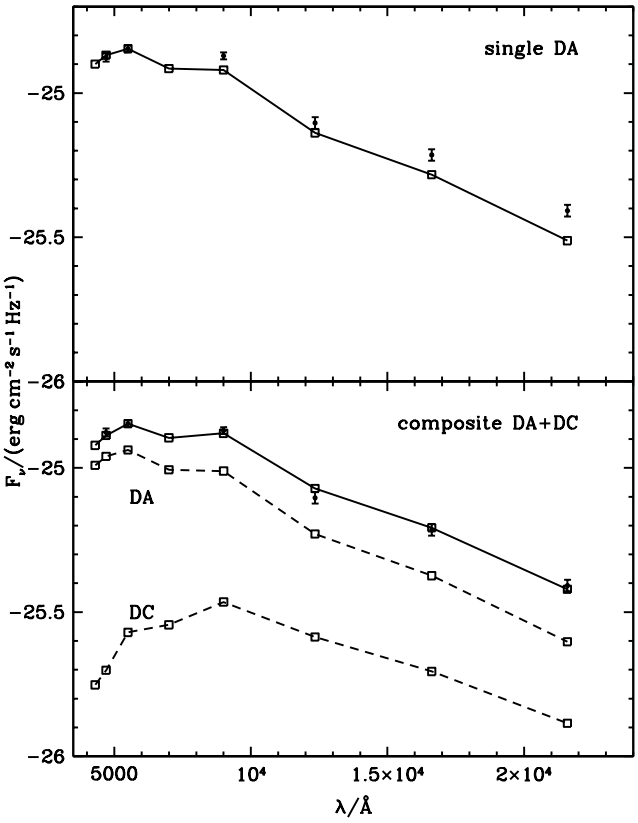

Fig. 4. *Top*: model flux of a 9300 K DA white dwarf compared to the observed fluxes (converted from magnitudes). For clarity we show only the *JHK* measurements of Bergeron et al. (2001). *Bottom*: comparison of the best fit composite DA+DC spectrum to the observed fluxes. The individual contributions of the DA and DC components are shown as dashed lines.

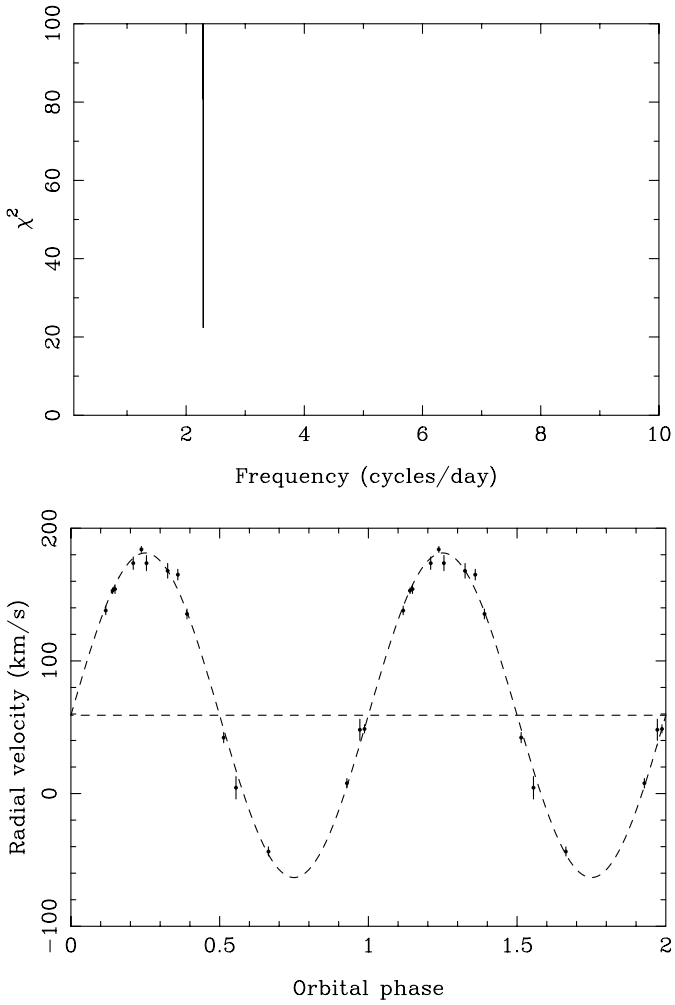

Fig. 5. Periodogram for WD1013−010 in cycles per day and data folded on the best fit period.

3.4. WD1013−010

WD1013−010 is a cool white dwarf (8000 K) with a mass of 0.44 $M_\odot$. The periodogram for WD1013−010 is plotted in Fig. 5. The best fit period is 0.437 d. The folded radial velocity curve is shown in Fig. 5. The next best period, with $\chi^2 = 51$ has virtually the same period and thus overlaps with the best fit period in Fig. 5.

3.5. WD1210+140

WD1210+140 is another hot white dwarf (32 000 K) of very low mass: 0.23 $M_\odot$. It is the lowest mass white dwarf known in a double white dwarf binary, and one of the lowest mass white dwarfs known. Interestingly, Maxted & Marsh (1999) observed WD1210+140 and, despite the large radial velocity amplitude of the system, concluded is is not a binary, but only based on two (consecutive) spectra. We included their two measurements (taken in 1998) in our fit. This results in a unique solution for the system, with orbital period of 0.64 d (Table 2). The radial velocity curve, folded on the best period is shown in Fig. 6. The measurements of Maxted & Marsh (1999) are included as open triangles. The mass of WD1210+140 is virtually identical to the mass of the sdB star in the 0.6 d binary HD 188112, in which the companion is a massive ($M > 0.73\ M_\odot$) compact object (Heber et al. 2003).

4. Is there any sign of the companions?

In order to search for signs of weak absorption lines of the companions, that potentially could be used to determine the mass ratio, we have to inspect the spectra around quadrature (phases 0.25 and 0.75) when the two spectra are most widely separated. In order to obtain high quality spectra to look for weak spectral features one generally combines spectra with similar phases. However, in general our single high singnal-to-noise ratio VLT survey spectra, that were used to measure the initial radial velocity offset are more suitable for this. In the survey spectra none of the systems discussed here showed any sign of absorption lines of the companion. Only for WD0326−273 we can improve on these results as many of the follow-up spectra were taken with the VLT as well. We therefore combined the VLT spectra in the phase range 0.15–0.35 (4 spectra) and 0.65–0.85 (9 spectra) after shifting out the radial velocities according to our best fit orbital solution. The resulting spectra are shown in Fig. 7, no additional absorption lines are seen, but see

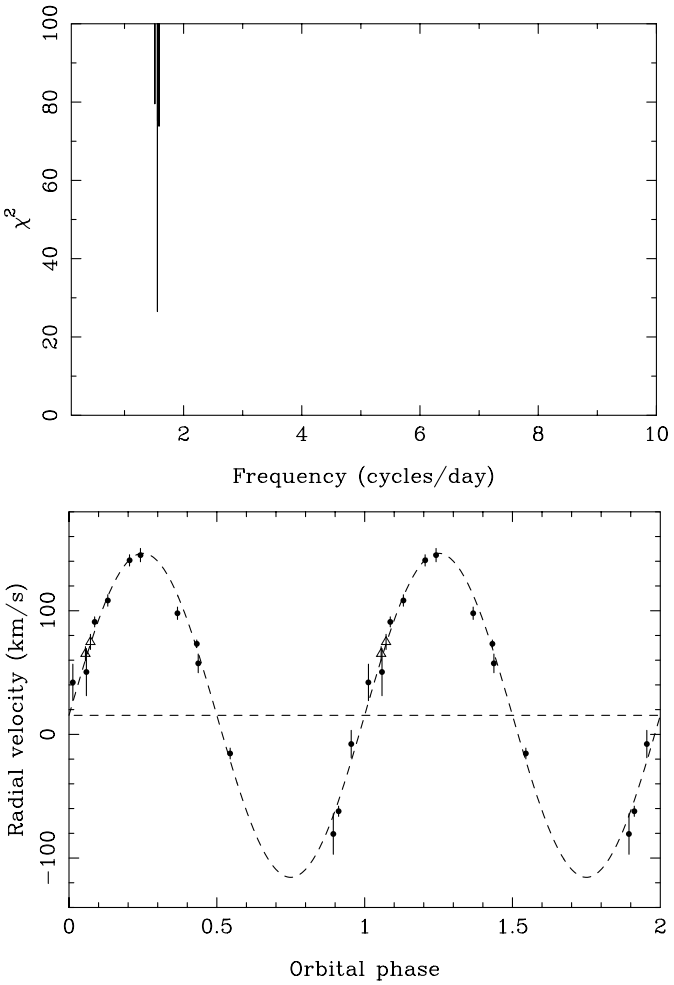

Fig. 6. Periodogram for WD1210+140 in cycles per day and data folded on the best fit period.

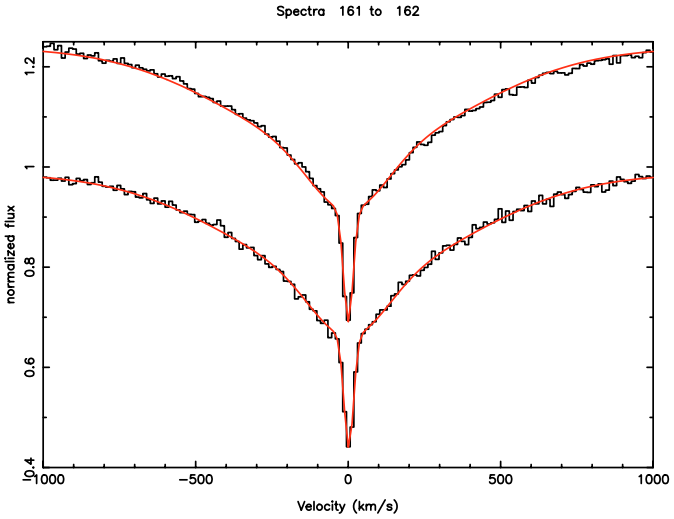

Fig. 7. Quadrature spectra of WD0326−273, after shifting out the best fit sinusoidal radial velocity curve and combining the spectra in the phase intervals 0.15–0.35 (*top*) and 0.65–0.85 (*bottom*). Any signs of the companion would show up as an asymmetry in these two spectra.

Sect. 3.3 for our arguments that there must be significant flux from a featureless companion.

5. Discussion

In total there are now 24 double white dwarfs known. The parameters of all systems are shown in Table 3, including the new systems discussed in this paper. Of the new systems WD0326−273 and WD1210+140 are particularly interesting, having rather high (0.51 $M_\odot$) and very low (0.23 $M_\odot$) masses respectively. The difference in the approach between the earlier work (targeting low-mass white dwarfs) and the SPY project is starting to become clear. Of the four clear C/O white dwarfs (taken as $M > 0.5\ M_\odot$) three were found by SPY. There are a few changes compared to earlier compilations like this (e.g. Maxted & Marsh 1999; Nelemans & Tout 2005), in particular some of the masses of the white dwarfs have been redetermined. There are also some small changes in the masses given in new papers (Maxted et al. 2002b; Morales-Rueda et al. 2005). In the table we also list the minimum companion star mass for the single-lined spectroscopic binaries, based on the mass function and assuming an inclination of 90 degrees. We can now use the above data in order to compare with theoretical models of the local population of double white dwarfs to see if the new systems change the conclusions of earlier comparisons. We compare the data with a slightly updated version of the population synthesis calculation of Nelemans et al. (2001), as detailed in Nelemans et al. (2004). Earlier population synthesis calculations for double white dwarfs are reported e.g. in Iben et al. (1997); Han (1998).

In Fig. 8 we plot the distribution in the period – white dwarf mass plane, for the brighter white dwarf in each binary (M_1). All observed double white dwarfs are plotted on top of the theoretical distribution for a magnitude limited sample with ($V < 20$). A few things should be noted before conclusions based on this diagram can be drawn. The most important is that the observed systems are not (yet) an unbiased sample. The SPY project will provide a much more unbiased sample, but only when the majority of the discovered binaries have known periods. More specific, the observed systems are still dominated by the low-mass white dwarfs that were targeted by Marsh and collaborators.

Taking the plot as it is, two things can be concluded. The first is that the new observations occupy similar regions in the diagram and thus conform to the general picture that was seen before and which can be explained adequately by the population synthesis calculations. It also confirms the earlier finding (Nelemans et al. 2001) that the lowest mass white dwarfs do not keep a thick hydrogen envelope in which residual burning continues, as was suggested by Driebe et al. (1998), which would predict many systems with very low masses (although WD1210+140 shows that some systems with $M < 0.25\ M_\odot$ do exist). This might be due to thermal instabilities in which the hydrogen is lost (e.g. Driebe et al. 1999). However, we currently use a cooling prescription based on the models of Hansen (1999), as detailed in Nelemans et al. (2004), which assume a constant hydrogen envelope mass as function of the mass of the white dwarf. This prescription enhances the presence of systems with masses above 0.5 $M_\odot$ in Fig. 8, as compared to the

Table 3. Properties of the observed double white dwarfs.

Object	P (d)	M_1 ($M_\odot$)	M_2 ($M_\odot$)	Ref
WD0135−052	1.56	0.47	0.52	1, 2
WD0136+768	1.41	0.47	0.37	8, 13
HE0320−1917	0.87	0.29	>0.35	18
WD0326−273	1.88	0.51	>0.59	18
WD0957−666	0.06	0.37	0.32	3, 7
WD1013−010	0.43	0.44	>0.38	18
WD1022+050	1.16	0.39	>0.28	8, 17
WD1101+364	0.15	0.29	0.35	4, 13
WD1115+166	30.09	0.52	0.43	12
WD1202+608	1.49	0.4	>0.34	6
WD1204+450	1.60	0.46	0.52	8, 13
WD1210+140	0.64	0.23	>0.38	18
WD1241−010	3.35	0.31	>0.37	5
WD1317+453	4.87	0.33	>0.42	5
WD1349+144	2.12	0.44	0.44	14
HE1414−0848	0.52	0.71	0.55	11, 15
WD1428+373	1.14	0.35	>0.23	9, 17
HE1511−0448	3.22	0.48	>0.46	18
WD1704+481	0.14	0.39	0.56	10
WD1713+332	1.12	0.35	>0.18	5
WD1824+040	6.27	0.43	>0.52	8, 17
WD2032+188	5.08	0.41	>0.47	8, 17
HE2209−1444	0.28	0.58	0.58	16
WD2331+290	0.17	0.39	>0.32	5

References: (1) Saffer et al. (1988); (2) Bergeron et al. (1989); (3) Bragaglia et al. (1990); (4) Marsh (1995); (5) Marsh et al. (1995); (6) Holberg et al. (1995); (7) Moran et al. (1997); (8) Maxted & Marsh (1999); (9) Marsh (2000) and P. Maxted, private communication; (10) Maxted et al. (2000b); (11) Napiwotzki et al. (2002b); (12) Maxted et al. (2002a); (13) Maxted et al. (2002b); (14) Karl et al. (2002); (15) Napiwotzki et al. (2002a); (16) Karl et al. (2003); (17) Morales-Rueda et al. (2005); (18) this paper.

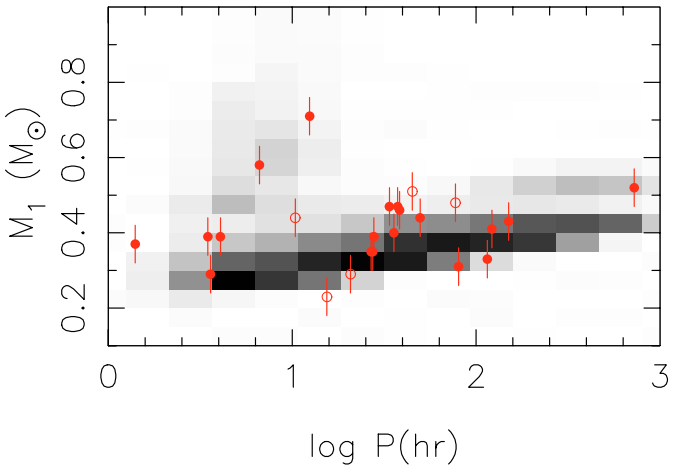

Fig. 8. Period–mass (M_1) distribution for double white dwarfs. The systems presented in this paper are shown with the open circles.

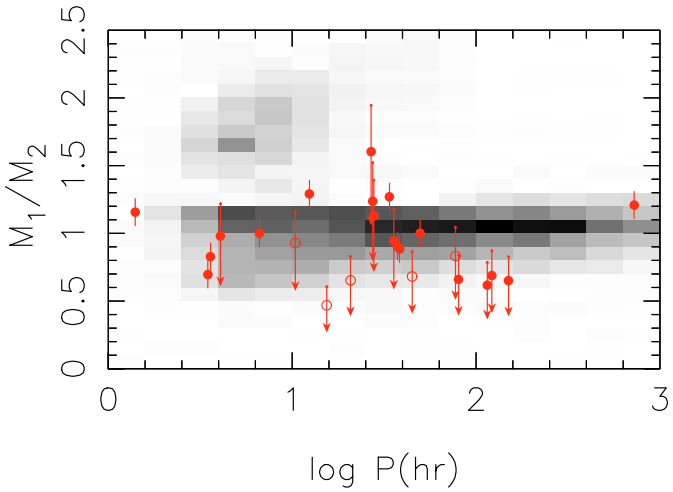

Fig. 9. Period–mass ratio (M_1/M_2) distribution for double white dwarfs. The systems presented in this paper are again shown with the open circles. The systems for which only a lower limit to the mass of the companion is know are shown with the arrows. They are drawn from the maximum mass ratio (for $M_2 = M_{2,\rm min}$), to the point where there is a 75 percent probability that the mass ratio lies above this point. The large circle is plotted at the position of the median inclination (60 degrees). Open circles again are the systems presented in this paper. In the theoretical distribution M_1 is selected to be the mass of the brightest object of the two (based on age and cooling, generally the second formed white dwarf).

same plot in Nelemans et al. (2001), more consistent with the observations. The second conclusion is that the apparent gap in the period distribution between 0.5 and 1 day, which was noted in Nelemans et al. (2001) indeed was due to small number statistics and is filling in.

In Table 3 we also included the minimum mass of the companion for the single-lined systems. The mass ratios of double white dwarfs[1] have led to the suggestion that the standard description of the common-envelope phase in close binaries needs revision (Nelemans et al. 2000). The population synthesis calculations of Nelemans et al. (2001) are based on this suggested revision. A recent reassessment of the need for this revision, based on the newly discovered double-lined double white dwarfs confirms the earlier findings (Nelemans & Tout 2005). In these analyses only double-lined systems were taken into account. However, in Fig. 9 we compare the theoretical distribution in the period–mass ratio (M_1/M_2) plane with all observations, where for the single-lined systems we show a plausible range of mass ratios, based on the mass limit on the companion star. For each system we plot an arrow that starts at the maximum mass ratio (for the minimum companion star mass, i.e. for 90 degrees inclination). The arrow extends to the mass ratio for an inclination of 41 degrees, which corresponds to a 75 percent probability that the actual mass ratio lies along the arrow. The large symbol is plotted at the mass ratio for the

[1] Traditionally taken to be the mass of the brighter over the mass of the dimmer component (M_1/M_2), e.g. Iben et al. (1997); Maxted et al. (2000b).

median for random orientations, i.e. an inclination of 60 degrees. In the theoretical distribution for each system the brightest of the two white dwarfs (in the V band) is determined, based on the age and the (mass dependent) cooling curve and its mass is taken as M_1. This generally is the second formed white dwarf.

Although the general agreement between the observations and the theory is good, it clearly is not as good for the single-lined systems as for the double-lined systems (shown as symbols with error bars), for which the theory was developed. In particular the mass ratios for the longer period systems seem to be lower than predicted. Detailed investigation of this discrepancy is beyond the scope of this paper.

Acknowledgements. G.N. is supported by NWO-VENI grant 639.041.405. C.K. was supported by DFG grants NA 365/3-1 and He 1356/40-3. R.N. acknowledges support by a PPARC Advanced Fellowship. Calar Alto observations were supported by DFG travel grants. R.G.I. thanks PPARC for a studentship, and CIQuA for a fellowship. GR is supported by NWO-VIDI grant 639.042.201. B.V. acknowledges support from the Deutsche Forschungsgemeinschaft (grant KO738/21-1).

References

Benvenuto, O. G., & Althaus, L. G. 1999, MNRAS, 303, 30
Bergeron, P., Wesemael, F., Fontaine, G., & Liebert, J. 1989, ApJ, 345, L91
Bergeron, P., Wesemael, F., & Beauchamp, A. 1995, PASP, 107, 1047
Bergeron, P., Leggett, S. K., & Ruiz, M. T. 2001, ApJS, 133, 413
Bessell, M. S., & Wickramasinghe, D. T. 1978, MNRAS, 182, 275
Bragaglia, A., Greggio, L., Renzini, A., & D'Odorico, S. 1990, ApJ, 365, L13
Christlieb, N., Wisotzki, L., Reimers, D., et al. 2001, A&A, 366, 898
Driebe, T., Schönberner, D., Blöcker, T., & Herwig, F. 1998, A&A, 339, 123
Driebe, T., Blöcker, T., Schönberner, D., & Herwig, F. 1999, A&A, 350, 89
Han, Z. 1998, MNRAS, 296, 1019
Hansen, B. M. S. 1999, ApJ, 520, 680
Heber, U., Edelmann, H., Lisker, T., & Napiwotzki, R. 2003, A&A, 411, L477
Hoeflich, P., Wheeler, J. C., & Thielemann, F. K. 1998, ApJ, 495, 617
Holberg, J. B., Saffer, R. A., Tweedy, R. W., & Barstow, M. A. 1995, ApJ, 452, L133
Iben, Jr, I., & Tutukov, A. V. 1984, ApJ, 284, 719
Iben, Jr, I., Tutukov, A. V., & Yungelson, L. R. 1997, ApJ, 475, 291
Karl, C., Napiwotzki, R., Heber, U., et al. 2002, in White Dwarfs, Proc. XIII Workshop on White Dwarfs, ed. D. de Martino, R. Kalytis, R. Silvotti, & J. Solheim (Kluwer), 43
Karl, C., Napiwotzki, R., Nelemans, G., et al. 2003, A&A, 410, 663
Koester, D. 1987, ApJ, 322, 852
Koester, D., Napiwotzki, R., Christlieb, N., et al. 2001, A&A, 378, 556
Leibundgut, B. 2001, ARA&A, 39, 67
Livio, M. 2001, in Supernovae and Gamma-Ray Bursts: the Greatest Explosions since the Big Bang, STScI Symp. Ser., 13, 334
Luyten, W. J. 1949, ApJ, 109, 528
Luyten, W. J. 1957, A catalogue of 9867 stars in the Southern Hemisphere with proper motions exceeding 0.″2 annually (Minneapolis, Lund Press)
Marsh, T. R. 1995, MNRAS, 275, L1
Marsh, T. R. 2000, New Astron. Rev., 44, 119
Marsh, T. R., Dhillon, V. S., & Duck, S. R. 1995, MNRAS, 275, 828
Maxted, P. F. L., & Marsh, T. R. 1999, MNRAS, 307, 122
Maxted, P. F. L., Marsh, T. R., & Moran, C. K. J. 2000a, MNRAS, 319, 305
Maxted, P. F. L., Marsh, T. R., Moran, C. K. J., & Han, Z. 2000b, MNRAS, 314, 334
Maxted, P. F. L., Burleigh, M. R., Marsh, T. R., & Bannister, N. P. 2002a, MNRAS, 334, 833
Maxted, P. F. L., Marsh, T. R., & Moran, C. K. J. 2002b, MNRAS, 332, 745
Morales-Rueda, L., Marsh, T., Maxted, P., et al. 2005, MNRAS, 359, 648
Moran, C. K. J., Marsh, T. R., & Bragaglia, A. 1997, MNRAS, 288, 538
Napiwotzki, R., Christlieb, N., Drechsel, H., et al. 2001a, Astronomische Nachrichten, 322, 411
Napiwotzki, R., Edelmann, H., Heber, U., et al. 2001b, A&A, 378, L17
Napiwotzki, R., Drechsel, H., Heber, U., et al. 2002a, in White Dwarfs, Proc. XIII Workshop on White Dwarfs, ed. D. de Martino, R. Kalytis, R. Silvotti, & J. Solheim (Kluwer), 39
Napiwotzki, R., Koester, D., Nelemans, G., et al. 2002b, A&A, 386, 957
Napiwotzki, R., Karl, C. A., Lisker, T., et al. 2004a, Ap&SS, 291, 321
Napiwotzki, R., Yungelson, L., Nelemans, G., et al. 2004b, in Spectroscopically and Spatially Resolving the Components of the Close Binary Stars (San Francisco: ASP), ASP Conf. Ser., 318, 402
Nelemans, G., & Tout, C. A. 2005, MNRAS, 356, 753
Nelemans, G., Verbunt, F., Yungelson, L. R., & Portegies Zwart, S. F. 2000, A&A, 360, 1011
Nelemans, G., Yungelson, L. R., Portegies Zwart, S. F., & Verbunt, F. 2001, A&A, 365, 491
Nelemans, G., Yungelson, L. R., & Portegies Zwart, S. F. 2004, MNRAS, 349, 181
Piersanti, L., Gagliardi, S., Iben, I. J., & Tornambé, A. 2003, ApJ, 583, 885
Saffer, R. A., Liebert, J., & Olszewski, E. W. 1988, ApJ, 334, 947
Saio, H., & Nomoto, K. 1998, ApJ, 500, 388
Saio, H., & Nomoto, K. 2004, ApJ, 615, 444
Webbink, R. F. 1984, ApJ, 277, 355
Wegner, G., & Reid, I. N. 1991, ApJ, 375, 674

Online Material

Appendix A: Radial velocity measurements

Table A.1. Radial velocity measurements of WD0326−273.

HJD −2 450 000	*RV* (km s^{-1})	Tel	HJD −2 450 000	*RV* (km s^{-1})	Tel
1737.9246	148.4 ± 0.8	V	2213.5416	−25.4 ± 2.7	I
1740.8767	−28.7 ± 0.7	V	2213.6239	−25.8 ± 2.6	I
2194.6455	−19.9 ± 0.5	V	2540.7119	161.3 ± 2.1	N
2194.6947	−24.5 ± 0.6	V	2540.7859	166.1 ± 1.8	N
2194.7268	−25.2 ± 0.5	V	2540.8050	165.9 ± 1.7	N
2194.7534	−25.3 ± 0.6	V	2541.7981	−26.8 ± 1.8	N
2194.7886	−25.3 ± 0.5	V	2541.8911	−16.4 ± 2.5	N
2194.8322	−22.4 ± 0.5	V	2542.6806	162.6 ± 1.6	N
2194.8820	−16.5 ± 0.4	V	2542.7960	156.7 ± 1.9	N
2195.6932	165.1 ± 0.6	V	2543.6692	−23.9 ± 1.9	N
2195.8242	162.3 ± 0.5	V	2543.7380	−14.2 ± 2.8	N
2209.5487	25.6 ± 5.8	I	2543.7790	−3.0 ± 3.0	N
2209.5967	−10.2 ± 2.5	I	2543.8676	5.0 ± 2.5	N
2209.6437	−13.4 ± 2.6	I	2589.7266	155.7 ± 0.5	V
2210.5780	157.7 ± 3.3	I	2590.5973	−20.4 ± 0.7	V
2210.6372	149.5 ± 3.0	I	2591.5698	159.4 ± 0.5	V
2211.5480	−25.7 ± 3.7	I	2592.5529	−7.7 ± 0.5	V
2211.6212	−27.5 ± 2.6	I	2592.6856	24.0 ± 0.5	V
2211.6706	−31.9 ± 3.9	I	2592.8506	72.6 ± 0.6	V
2212.5297	150.0 ± 7.4	I			

Table 2. Radial velocity measurements of HE0320−1917, HE1511−0448, WD1013−010 and WD1210+140.

HJD −2 450 000	*RV* (km s^{-1})	Tel	HJD −2 450 000	*RV* (km s^{-1})	Tel	HJD −2 450 000	*RV* (km s^{-1})	Tel	HJD −2 450 000	*RV* (km s^{-1})	Tel
HE0320−1917			**HE1511−0448**			**WD1013−010**			**WD1210+140**		
1946.6477	87.1 ± 3.5	V	1701.7312	−67.2 ± 3.0	V	2663.7956	184.0 ± 1.1	V	0969.8965	65.2 ± 5.4	W
1947.6129	14.7 ± 1.4	V	2078.6244	−62.6 ± 2.4	V	2684.7070	152.9 ± 0.8	V	0969.9073	74.8 ± 5.8	W
2589.5967	−52.8 ± 1.2	V	2097.4761	−4.0 ± 11.1	C	3337.8448	167.9 ± 5.2	N	2657.8067	73.3 ± 2.3	V
2591.7642	147.6 ± 1.4	V	2099.4753	−31.1 ± 9.1	C	3337.8597	165.0 ± 3.5	N	2658.7567	−62.2 ± 3.6	V
2592.6408	145.4 ± 2.9	V	2328.6753	35.3 ± 5.7	C	3338.8658	−43.6 ± 2.8	N	2747.4391	50.4 ± 19.0	C
2592.7861	59.4 ± 1.9	V	2329.6789	−17.1 ± 6.2	C	3339.8540	7.8 ± 3.0	N	2747.5327	140.7 ± 4.1	C
2662.3474	−23.1 ± 3.8	W	2431.5274	−1.3 ± 2.9	V	3339.8730	48.1 ± 7.7	N	2748.3933	−15.5 ± 3.9	C
2662.4120	20.0 ± 3.0	W	2431.5693	5.3 ± 2.9	V	3340.8233	154.1 ± 2.6	N	2749.3355	42.1 ± 14.6	C
2663.3955	103.1 ± 2.3	W	2431.6163	14.4 ± 3.0	V	3340.8695	173.7 ± 5.3	N	2749.4113	108.3 ± 4.2	C
2663.4130	115.1 ± 2.5	W	2663.7524	21.2 ± 9.1	W	3341.8019	135.4 ± 3.1	N	2749.4823	145.0 ± 5.0	C
2663.4306	135.0 ± 2.6	W	2717.8675	−59.9 ± 3.9	V	3341.8558	42.2 ± 3.3	N	2749.5628	98.0 ± 4.6	C
2664.3339	143.2 ± 3.6	W	2721.6133	4.7 ± 6.7	W	3341.8739	4.4 ± 8.2	N	2750.5431	−80.5 ± 16.3	C
3344.5901	−49.4 ± 10.4	W6	2825.4342	8.3 ± 11.8	C	3344.7788	173.6 ± 4.3	W	2750.5818	−7.8 ± 10.9	C
3369.4729	65.6 ± 3.4	W	2826.4060	−85.3 ± 9.5	C	3365.6354	48.8 ± 2.4	W	2773.3597	57.4 ± 7.3	C
3370.4654	−30.3 ± 3.4	W	2837.4181	−26.0 ± 13.4	C	3368.7479	138.0 ± 2.6	W	3370.7838	91.0 ± 3.5	W